Hindered and modulated rotations of adsorbed diatomic molecules: States and spectra

Uzi Landman, G. G. Kleiman,* C. L. Cleveland, E. Kuster, R. N. Barnett
School of Physics, Georgia Institute of Technology, Atlanta, Georgia 30332

J. W. Gadzuk
National Bureau of Standards, Washington, D.C. 20234
(Received 20 October 1983)

We present results for the rotational states and spectra of adsorbed diatomic molecules whose rotations are frustrated by the interaction with the substrate, for several solvable models of the interaction potentials. For a vertical adsorption configuration, hindrance is modeled by constraining the molecular motion via an infinite conical potential well. For a horizontal adsorption configuration the infinite conical-well model as well as hindrance caused by a softer hindrance potential are studied. For both hindrance models we study the effects caused by a modulation of the molecular motion due to periodic azimuthal potentials dependent upon the adsorption site symmetry and other characteristics of the adsorption system. A detailed analysis of the spectra as a function of the parameters of the models is presented, allowing us to formulate a state classification scheme and draw general conclusions with regard to the systematics of the spectra of frustrated rotations of adsorbed diatomic molecules applicable to a wide class of potentials, which could guide the analysis and interpretation of data.

I. INTRODUCTION

Knowledge of the eigenstates and spectra of physical systems is a fundamental element in understanding their physical properties, the nature of their interactions, and a prerequisite for investigations of dynamical processes. The interaction of atoms and molecules with solid surfaces is characterized by potentials and boundary conditions which, depending on the particular solid and molecular species involved and on ambient conditions (such as temperature), can (and often do) alter significantly the spectra of the separated systems. The recent development and application of experimental techniques [such as high-resolution electron-loss spectroscopy (HREELS),[1] surface infra-red spectroscopy,[2] surface neutron scattering measurements,[3] and laser-induced fluorescence[4(a)]] provide detailed spectroscopic information about the vibrational and rotational states of adsorption systems and the internal states distributions of scattered, desorbed, or ejected molecules.[4(b)] Analysis of such spectroscopic data of adsorption systems could yield information about the underlying substrate-adsorbate potential-energy surfaces, adsorption configurations, and the nature of the adsorbate motional degrees of freedom. Since at this stage of development accurate knowledge about molecule-surface interaction potential surfaces is rather sparse, it is fruitful and timely to investigate simple soluble models which incorporate the essential physical elements, allow systematic investigations, and permit understanding of the system in terms of basic physical concepts. While in the present study we explore the rotational states of molecules adsorbed on solid surfaces, the concepts and method of analysis which we introduce can be generalized in a rather straightforward manner to investigations of the rotational spectroscopy[5] of diatomic molecules in solid matrices.

Motivated by the above considerations, we introduce in this paper several exactly soluble models of the rotational motion of an adsorbed diatomic molecule and analyze their solutions in an attempt to demonstrate some of the effects which the molecule-surface interaction could have on the rotational spectrum of the admolecule. In the limit of a weak interaction with the substrate (physisorption), one expects free rotational motion of the molecule[1] (particularly on close-packed surfaces) while for stronger interactions, hindrance (frustration) of the rotations is expected.[6,7] The manner and degree in which the substrate may influence the rotations of the admolecule will depend on characteristics of the adsorption system potential surface which, in turn, depends on the adsorption site local symmetry and on the adsorbed molecule configuration. In our study we consider the rotational motion of diatomic molecules whose equilibrium adsorption configuration is either vertical or horizontal with respect to the surface. For the case of vertical adsorption we solve for the rotational eigenstates and spectra of a molecule whose motion is hindered by an infinite conical well and investigate the changes in the rotational eigenstates as the degree of hindrance (opening angle of the conical well) is varied. For an adsorption system where, in equilibrium, the internuclear axis of the admolecule is parallel to the surface we consider two possible hindrance potentials: an infinite conical well which restricts the molecule to a finite volume and a "softer" hindrance potential which turns on gradually as the molecule deviates from its equilibrium configuration. In addition, for such horizontal adsorption configurations we study the effect of periodic azimuthal modulation of the rotational motion due to the local symmetry of the potential surface about the adsorption site.

We present a detailed analysis of the hindered and/or moldulated rotational states of the admolecule as a function of the model parameters (degrees of hindrance and modulation, site geometry, and types of hindrance potentials), which allows us to reach a state classification scheme and draw general conclusions with regard to the systematics of the states as a function of the potential parameters which should hold for a wide class of potentials. In addition we suggest a systematic prescription for the extraction of the band structure associated with the periodic azimuthal potential from experimental data.

A description of our models and their analytical solutions are presented in Sec. II. Results of calculations which demonstrate the spectroscopic consequences of our model interaction potentials and a systematic classification scheme for the corresponding admolecule rotational states are adduced in Sec. III. The incorporation of these results, and their consequences, in model calculations of the internal state distributions of desorbed molecules have been discussed by us previously for a certain class of our models[6] and will be reported in detail in a planned subsequent publication.

II. MODELS AND SOLUTIONS

In Fig. 1 we illustrate schematically the constraints imposed by a solid surface upon the rotational motion of a diatomic molecule chemisorbed either vertically or horizontally with respect to the surface plane. The primary effects of the surface are those of hindering the motion of the adsorbed molecule, or restricting the volume in which the molecule rotates, and of possibly introducing a dependence upon site local geometry via an azimuthal modulation of the molecular motion (Fig. 2). The Schrödinger equation for such rotations is given in spherical coordinates by

$$\left[-\frac{1}{2I}L^2(x,\phi)+U(x,\phi)-\frac{\hbar^2\nu(\nu+1)}{2I}\right]\psi_{\nu\mu}(x,\phi)=0\ , \quad (1a)$$

$$L^2(x,\phi)\equiv\hbar^2\left[\frac{\partial}{\partial x}\left[(1-x^2)\frac{\partial}{\partial x}\right]+\frac{1}{1-x^2}\frac{\partial^2}{\partial\phi^2}\right]\ , \quad (1b)$$

where $x\equiv\cos\theta$, and $\psi_{\nu\mu}$ is normalized,

$$\int_{-1}^{1}dx\int_{0}^{2\pi}d\phi\,|\psi_{\nu\mu}|^2=1\ . \quad (1c)$$

The polar angle θ is defined with respect to the outward surface normal, the quantity I is the molecule's moment of inertia with respect to its center of rotation, U is the potential energy of interaction with the surface, and the last term in Eq. (1a) represents the energy in a form which makes an obvious connection with the limit of free rotations. The quantity μ represents other quantum numbers arising from the dependence of U upon the azimuthal angle ϕ.

In accordance with our stated objective of modeling the system by a solvable model we express U in the unique form which permits separation of variables:[8]

$$U(x,\phi)=\left[W(x)+\frac{V(\phi)}{1-x^2}\right]\frac{\hbar^2}{2I}\ . \quad (2)$$

From here on energies and potentials are in units of $\hbar^2/2I$. With U given by Eq. (2), the wave function can be factored as

$$\psi_{\nu\mu}(x,\phi)=P_\nu^\mu(x)\Phi_\mu(\phi)\ , \quad (3a)$$

where the functions $\Phi_\mu(\phi)$ and $P_\nu^\mu(x)$ are the solutions to

$$\left[\frac{d^2}{d\phi^2}+\mu^2-V(\phi)\right]\Phi_\mu(\phi)=0\ , \quad (3b)$$

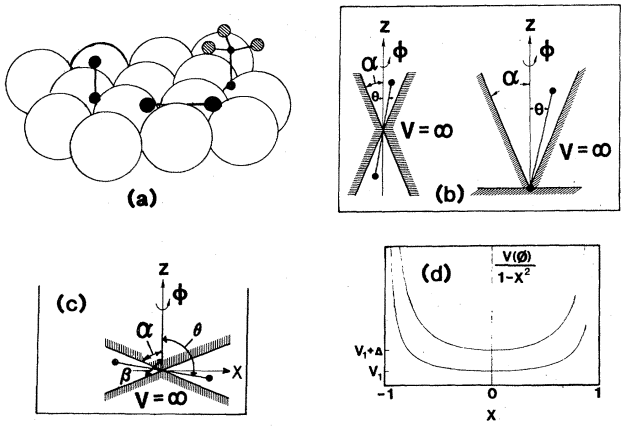

FIG. 1. (a) Schematic picture of molecular adsorption systems in which hindrance and/or modulation of the admolecule motion may occur. The adsorbed diatomic molecules at the left and center differ in their equilibrium adsorption configuration (vertical and horizontal, respectively). (b) Schematics of the infinite cone-well hindrance model for vertical adsorption configuration (v model). The molecular rotations are restricted to a conical sector of opening polar angle α. (c) Schematic of the infinite cone-well hindrance model for horizontal adsorption configuration (h model). The molecular rotations are restricted to a conical sector defined by the angles α and β. (d) Schematic of the h_2 hindrance model, for horizontal adsorption configuration. In the figure $x=\cos\theta$ where θ is the polar angle measured from the normal to the surface and the two curves correspond to the $V(\phi)$ defined by Eq. (9) in the text.

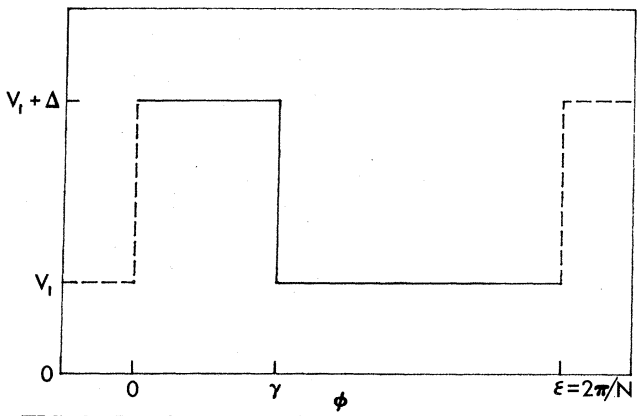

FIG. 2. Kronig-Penney azimuthal modulation potential [see Eq. (9)]. N is the symmetry number (periodicity), Δ is the height of the modulation barrier, and γ is the width of the barrier.

and

$$\frac{d}{dx}\left[(1-x^2)\frac{dP_\nu^\mu(x)}{dx}\right] + \left[\nu(\nu+1)-\frac{\mu^2}{1-x^2}-W(x)\right]P_\nu^\mu(x)=0\ . \quad (3c)$$

In the limit $V\to 0$, $\Phi\sim e^{im\phi}$, where m is an integer since single valuedness dictates $\Phi(\phi)=\Phi(\phi+2\pi)$, and Eq. (3c) reduces to Legendre's equation for $W=0$.

We first model the hindrance of the molecular rotation by constraining its motion about the polar angle to conical volumes of rotation [see Figs. 1(b) and 1(c)]. The forms of potentials $W(x)$, see Eq. (2), corresponding to this model of hindrance for vertical (i.e., v) and horizontal (i.e., h) configurations of the adsorbed molecule are [using the angle conventions in Figs. 1(b) and 1(c)]

$$W_v(x)\equiv \lim_{C\to\infty} C\theta(\cos(\alpha)-x)\ , \quad (4a)$$

$$W_h(x)= \lim_{C\to\infty} C[\theta(x-\cos\alpha)+\theta(\cos(\beta)-x)]\ , \quad (4b)$$

where $\theta(t)$ is defined as

$$\theta(t)= \lim_{\delta\to 0^+}\frac{1}{2}\left[1+\frac{t-\delta}{|t|+\delta}\right]\ . \quad (4c)$$

The potentials W_v (Ref. 6) and W_h describe infinite square wells in the variable x, and α and β are opening angles of the cone as defined in Fig. 1(c).

A few comments are in order regarding the form of the potential in Eq. (2). The term $V(\phi)/(1-x^2)$ has a minimum for $x=0$ and diverges as $|x|\to 1$, as illustrated in Fig. 1(d). We choose to include such a potential term only for horizontally adsorbed molecules and we omit it in our studies of the vertical adsorption configuration (i.e., $\mu=m$ where m is an integer for the v model). As illustrated in Fig. 1(d), we can simulate the effects of hindrance by choosing the magnitude of $V(\phi)$ appropriately, since the rotor does not penetrate readily into classically forbidden regions.

Our second model of hindered rotation of a horizontally chemisorbed molecule, denoted by h_2, is simply that of neglecting the polar hindrance potential $W(x)$ in Eq. (2) (e.g., no conical well) while retaining a modulating potential $V(\phi)$ which as discussed above can serve as a hindrance of the polar motion.

In order to facilitate discussion of the physical properties of our model potential in Eq. (2) and the relation to previous work,[6] we first present the solutions of the v, h, and h_2 models. The eigenvalue equation of the v model is given by

$$P_\nu^m(\cos\alpha)=0\ , \quad (5a)$$

where m is an integer and P_ν^m denotes the regular solution of Legendre's equation.[8] The eigenfunctions obey

$$\psi_{\nu m}(\theta,\phi)=A_{\nu m}(2\pi)^{-1/2}P_\nu^m(x)e^{im\phi}\theta(\cos(\alpha)-x)\ , \quad (5b)$$

with[6]

$$A_{\nu m}\equiv\left[-\frac{\nu+m}{2\nu+1}P_{\nu-1}^m(\cos\beta)\frac{d}{d\nu}P_\nu^m(\cos\alpha)\right]^{-1/2}\ . \quad (5c)$$

The h model involves a geometry complementary to that of the v model, as in Fig. 1(c), with the dispersion relation of the eigenvalues obeying,

$$L_{\nu\mu}(\cos\beta)\equiv P_\nu^\mu(\cos\alpha)Q_\nu^\mu(\cos\beta) - P_\nu^\mu(\cos\beta)Q_\nu^\mu(\cos\alpha)=0\ , \quad (6a)$$

where the opening angles α and β are defined in Fig. 1(c), μ^2 is the eigenvalue of Eq. (3b) [the solutions of our model for $V(\phi)$ are described in our Eqs. (8)–(11)], and Q_ν^μ represents the irregular solution of Legendre's equation.[8] The corresponding eigenfunctions are given by

$$\psi_{\nu\mu}(\theta,\phi)=B_{\nu\mu}[P_\nu^\mu(\cos\alpha)Q_\nu^\mu(x) - Q_\nu^\mu(\cos\alpha)P_\nu^\mu(x)]\Phi_\mu(\phi)\ , \equiv B_{\nu\mu}L_{\nu\mu}(x)\Phi_\mu(\phi)\ , \quad (6b)$$

where Φ_μ represents the normalized eigenfunction of Eq. (3b) [see Eq. (11) below] and the normalization factor $B_{\nu\mu}$ satisfies

$$B_{\nu\mu}\equiv\left[(2\nu+1)P_\nu^\mu(\cos\beta)\Big/\left[\frac{\partial}{\partial\nu}[L_{\nu\mu}(\cos\beta)P_\nu^\mu(\cos\alpha)W_{\nu\mu}]\right]\right]^{1/2}\ , \quad (6c)$$

with the Wronskian $W_{\nu\mu}$ defined by[8]

$$W_{\nu\mu}\equiv(1-x^2)\left[Q_\nu^\mu(x)\frac{d}{dx}P_\nu^\mu(x)-P_\nu^\mu(x)\frac{d}{dx}Q_\nu^\mu(x)\right]\ , \quad (6d)$$

$$=-\frac{2^{2\mu}\Gamma\left[1+\frac{(\nu+\mu)}{2}\right]\Gamma[\frac{1}{2}(1+\nu+\mu)]}{\Gamma[1+\frac{1}{2}(\nu-\mu)]\Gamma[\frac{1}{2}(1+\nu-\mu)]}\ . \quad (6e)$$

The solutions of the h_2 model, where we have no restrictive cone, are much simpler, since, for a given μ, the eigenvalues ν obey[8]

$$\nu=|\mu|+n,\quad n=0,1,2,\ldots, \quad (7a)$$

and the respective eigenfunctions satisfy

$$\psi_{\nu\mu}(\theta,\phi)=C_{\nu\mu}P_\nu^{-|\mu|}(x)\Phi_\mu(\phi)\ , \quad (7b)$$

$$C_{\nu\mu}\equiv\left[(\nu+\tfrac{1}{2})\frac{\Gamma(1+\nu+|\mu|)}{\Gamma(1+\nu-|\mu|)}\right]^{-1/2}\ . \quad (7c)$$

The choice of P_ν^μ, $\mu<0$, in Eq. (7b) derives from requirements of regularity at $x=\pm 1$; these requirements produce the eigenvalue spectrum in Eq. (7a), which, therefore, is seen to result from the boundary conditions in the same way as the spectra for the v and h models [i.e., Eqs. (5a) and (6a), respectively].

In our treatment of the azimuthal motion [see Eq. (3b)]

we consider an adsorbed molecule bound at a site such that the potential which the molecule feels due to the environment causes a periodic modulation of its motion. Thus, for our h models,

$$V(\phi+n\epsilon)=V(\phi),\quad \epsilon\equiv 2\pi/N\ , \tag{8a}$$

where n and N are integers, the latter characterizing the rotational periodicity of the site (i.e., twofold, fourfold, etc.). From the Floquet-Bloch theorem, and the property of single valuedness [i.e., $\Phi_\mu(\phi+2\pi)=\Phi_\mu(\phi)$], we have

$$\Phi_\mu(\phi)=e^{im\phi}U_\mu(\phi)\ , \tag{8b}$$

where m is an integer and $U_\mu(\phi+\epsilon)=U_\mu(\phi)$.

From Eqs. (3b) and (8), it is clear that the azimuthal motion corresponds to that of a particle moving in a one-dimensional periodic potential with periodic boundary conditions, which is a standard problem. Since we are interested here in determining the physical effects of a modulating potential, we model it by perhaps the simplest such periodic potential, a Kronig-Penney[9] model potential (see Fig. 2) whose value in the nth unit cell is

$$\begin{aligned} V(\phi)&=V_1+\Delta,\quad \epsilon-\gamma\le\phi-n\epsilon\le\epsilon \\ &=V_1\ ,\quad 0<\phi-n\epsilon<\epsilon-\gamma \end{aligned} \tag{9}$$

defining the azimuthal origin, and we let $\Delta\ge 0$ (i.e., a barrier of width γ). Choosing $\Delta=0$, and $V_1\neq 0$ and setting $W(x)=0$ in Eq. (2) corresponds to a horizontally adsorbed molecule whose unmodulated motion is hindered in the polar direction by the potential $V_1/(1-x^2)$ (i.e., the unmodulated h_2 model), while when $W(x)=0$, $\Delta\neq 0$, and $V_1\neq 0$ the modulated h_2 model is obtained. In our calculations of the modulated h model we set $V_1=0,\Delta\neq 0$ and hindrance is provided by W_h [see Eq. (4b)]. The eigenvalues of Eq. (3b) corresponding to the wave function in Eq. (8b) are given by the transcendental equation

$$\begin{aligned} 2\cos m\epsilon=\frac{1}{kK}\{&(K^2-k^2)\sin[k(\epsilon-\gamma)]\sinh(K\gamma) \\ &+2kK\cos[k(\epsilon-\gamma)]\cosh(K\gamma)\}\ , \end{aligned} \tag{10a}$$

$$K^2=\Delta-k^2\ , \tag{10b}$$

$$k^2=\mu^2-V_1\ . \tag{10c}$$

Equations (10) apply for $k^2\le\Delta$ (i.e., below the barrier). The corresponding expression for $k^2\ge\Delta$ can be derived by letting $K\to iK$.

The corresponding wave functions take the form, in the first unit cell, for $k^2\le\Delta$,

$$\Phi_\mu(\phi)=S_\mu[r_\mu f_\mu(\phi)+f_\mu^*(\phi)]\ , \tag{11a}$$

$$f_\mu(\phi)=\exp(ik\phi)\ ,\quad 0\le\phi\le\epsilon-\gamma \tag{11b}$$

$$=A(K,k)e^{K\phi}+A(-K,k)e^{-K\phi}\ ,\quad \epsilon-\gamma\le\phi\le\epsilon\ , \tag{11c}$$

where

$$A(K,k)\equiv e^{(K-ik)\gamma}\frac{(K+ik)}{2K}=A^*(K^*,-k)\ , \tag{11d}$$

$$r_\mu\equiv -F_\mu(K,k)/F_\mu(K,-k)\ , \tag{11e}$$

with

$$F_\mu(K,k)\equiv A(K,-k)+A(-K,-k)-e^{im\epsilon}e^{ik\epsilon}\ . \tag{11f}$$

The normalization factor S_μ is

$$S_\mu=[N(I_A+I_B)]^{-1/2}\ , \tag{11g}$$

where

$$\begin{aligned} I_A\equiv(\epsilon-\gamma)(1+|r_\mu|^2)& \\ +\frac{2}{k}\mathrm{Re}\{r_\mu e^{-ik(\epsilon+\gamma)}&\sin[k(\epsilon-\gamma)]\}\ , \end{aligned} \tag{11h}$$

$$I_B\equiv G(K)+G(-K)\ , \tag{11i}$$

$$G(K)\equiv\gamma C(K)C^*(-K)+\frac{|C(K)|^2}{2K}(1-e^{-2K\gamma})\ , \tag{11j}$$

$$C(K)\equiv r_\mu A(K,k)+A(K,-k)\ . \tag{11k}$$

The corresponding quantities for $k^2\ge\Delta$ can be derived from Eqs. (11) simply by making the correspondence $K\to iK$, and the complex-conjugate relation in Eq. (11d) holds as well for imaginary K. A general result for problems of this type is that the eigenvalues and eigenfunctions in Eq. (10) and (11) are independent of the absolute value of the minimum potential, here V_1: that is, they involve $k^2=\mu^2-V_1$ in our problem. Equations (6) and (7) for the polar angle quantities, on the other hand, involve k^2+V_1.

Insight into the meaning of the term $V(\phi)/(1-x^2)$ can be derived by treating a rigid diatomic molecule of internuclear separation r bound horizontally a distance z_0 above a solid plane, which, for simplicity, we first assume to be isotropic for azimuthal motion. For small oscillations[7] (small x) about one of the ends, the potential energy of the admolecule can be expanded in small deviations from the equilibrium configuration,

$$U(z_0+rx)\cong U(z_0)+\frac{1}{2}\left[\frac{d^2U(z_0)}{dz^2}\right]r^2x^2 \tag{12a}$$

$$\cong\left[U(z_0)-\frac{r^2}{2}\frac{d^2}{dz^2}U(z_0)\right]+\frac{1}{2}\left[\frac{d^2U(z_0)}{dz^2}\right]\frac{r^2}{1-x^2}\ . \tag{12b}$$

The quantity r is the length of the molecule (assumed rigid here) and a similar, but more complicated, expression results from considering an arbitrary point of support. Equation (12b) derives from the expansion of $(1-x^2)^{-1}$ for small x^2. An expression identical to Eq. (12a) was treated by White and Lassettre[7] for the study of ortho-para H_2 separation at solid surfaces. The relation between Eq. (12b) and the model potential in Eq. (2) permits us, for small x, to interpret the constant potential term [e.g., V_1 in Eqs. (9)–(11)] as a force constant governing polar angle oscillations about the equilibrium configuration. The inclusion of ϕ-dependent potential terms in Eqs. (12) would correspond to modulation of the azimuthal motion. Within this interpretation, the $(1-x^2)^{-1}$ factor in Eqs. (2)

and (12b) when x is allowed to take all values ($|x| \leq 1$), can be regarded as a simulation of hindrance of the polar motion beyond the harmonic approximation.

In order to make a closer connection with the work of White and Lassettre,[7] we consider the eigenvalue spectrum of Eq. (7a) for the case of $V_1 \neq 0$ and no modulating potential [i.e., $\Delta=0$ in Eq. (9)] so that $\mu^2=m^2+V_1$ with m an integer. Under these conditions, we have

$$\nu(\nu+1)-V_1=m^2+(2n+1)(V_1+m^2)^{1/2}+n(n+1) \quad (13a)$$

$$\underset{V_1\to\infty}{\to} m^2+(2n+1)\sqrt{V_1}+n(n+1)\,. \quad (13b)$$

As $V_1 \to 0$, $\nu \to l$, where l is the angular momentum of the free rotor. Then since Eq. (7a) holds for arbitrary V_1, we can make the identification $n=l-m$. In the limit of $V_1 \to \infty$, for fixed n, the energy spacings are those of a plane rotor[10] [whose energy equals $(\hbar^2/2I)m^2$], as in previous work.[7] For fixed m and $n \ll \sqrt{V_1}$, the energy spacings are those of a harmonic oscillator of force constant $\hbar^2 V_1/I$, in agreement with Eq. (12a). Finally, we should note, from Eq. (13a) that hindrance of the rotation persists for all states even for small V_1.

III. RESULTS AND DISCUSSION

For the analysis of experiments in which frustrated rotation of an adsorbed molecule may be probed, it is of importance to be able to interpret the measured spectra in terms of models of the molecule's rotational potential energy. In this section, we first discuss the physical interpretation of the energy spectra calculated for our various hindrance models in the absence of modulation, and then describe the effect of azimuthal modulation of the rotational motion. In order to facilitate interpretation of experimental spectra, we emphasize, throughout the presentation, discussion of those features of the calculated spectra which are model independent, delineation of those characteristics whose interpretations are unambiguous, and discrimination of the effects of hindrance and azimuthal modulation.

In Fig. 3(a), we present results of calculations of the rotational quantum number ν as a function of the opening angle α for the v model [i.e., see Fig. 1(b) for definitions of our conventions] considered previously.[6] From this figure, it is clear that increasing rotational hindrance (i.e., increasing spatial localization) increases ν (i.e., increases the kinetic energy), in such a fashion that the order of the displayed eigenvalues is maintained (i.e., there is no level crossing) throughout the angular range presented (i.e., from constraint to a half-space to nearly complete frustration). The states for $\alpha=\pi/2$ (i.e., half-space constraint) are just those free rotor solutions for which $l \pm m$ is odd (i.e., only odd P_l^m vanish on the midplane) and the evolution of these states with increasing frustration is illustrated. The azimuthal quantum number m is always conserved for these states, but ν is not an integer, except for special cases.[11(a)] Consideration of a larger hindrance angular range and higher rotational quantum numbers than those shown introduces complications (such as level crossings). A fuller treatment of these features is presented elsewhere.[11]

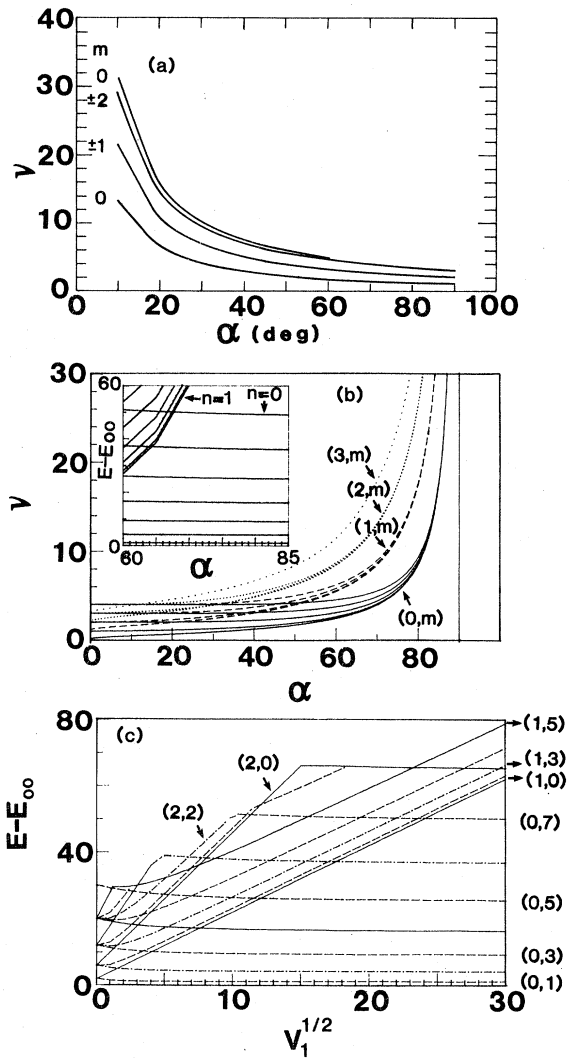

FIG. 3. (a) Rotational quantum number ν of a vertically hindered rotor vs the cone opening angle α (v model). The four lowest states are designated by the azimuthal quantum number m. (b) The rotational quantum number ν of an azimuthally unmodulated, horizontally hindered rotor (h model) vs the cone opening angle α (in degrees) with $\beta=180°-\alpha$ [see Fig. 1(c)]. The families of states are designated by (n,m) where $n=l-m$ and l is the rotation quantum number in the limit of a free rotor ($\alpha=0$). States in the first four families ($n=0,1,2,3$) are shown with the azimuthal quantum numbers in each family taking the sequential values $0,1,2,\ldots$, in one to one correspondence to the order of the energies (ν) in each family. The convergence of the states in each family, as the hindrance increases (increasing α), to two-dimensional rotor states is shown and further exhibited in the inset where the energy differences $E-E_{00} \equiv \nu(\nu+1) - \nu_{00}(\nu_{00}+1)$ vs α for $\alpha \geq 60°$ are displayed. A plane rotor spectrum is evident for the $n=0$ and 1 families. Note the rather large range of α for which the planar rotor behavior is obtained. (c) Energy differences $E-E_{00}$ vs $V_1^{1/2}$ (in units of $\hbar^2/2I$) for the unmodulated h_2 hindrance model. States are designated by $(n=l-m,m)$ where l is the rotational quantum number in the limit $V_1=0$ (i.e., free rotor). States corresponding to different n's belong to different families. The different families are distinguished by their asymptotic slopes [see also inset to (b)]. The plane rotor spectrum, is manifested for a wide range of V_1 values (larger range for the lower families).

Corresponding results for ν for the symmetric h model [i.e., $\alpha=\pi-\beta$ in Fig. 1(b)] without azimuthal modulation are illustrated in Fig. 3(b), where α runs the gamut from nearly total hindrance (i.e., $\alpha=\pi/2$) to free rotation (i.e., $\alpha=0$); in all the h-model results presented, we set $V_1=0$ in Eqs. (9) and (10c). As in our previous discussion, the rotational quantum numbers increase with increasing spatial localization. For intermediate values of α, the levels change their order from that of the free rotor and the separation of the levels into families as $\alpha\to\pi/2$ is clear, where all members of a family correspond to a common value of $l-m$ (i.e., $\nu\to l$ as $\alpha\to 0$), and the energies of the families have the same order as the values of $l-m$. Each family comprises the spectrum of the plane rotor, which can be appreciated from the inset in Fig. 3(b), where we plot the energy difference $E-E_{00}\equiv\nu(\nu+1)-\nu_{00}(\nu_{00}+1)$ in the region of $\alpha\geq\pi/3$ for the lowest two families and ν_{00} characterizes the ground state. The m^2 free plane rotor spectrum is obvious.

In order to motivate our discussion of the spectra classification scheme we examine the behavior of the h model as $\alpha\to\pi/2$. Transformation of the differential equation (3c) [with $W=W_h$ in Eq. (4b)] to one involving angles defined from the midplane, $\rho\equiv\pi/2-\theta$, $\xi\equiv\pi/2-\alpha=\beta-\pi/2$ (i.e., symmetric cone), and $H_{\nu\mu}(\rho)\equiv\sqrt{\cos\rho}P_\nu^\mu(\cos\theta)$ yields

$$\frac{d^2H_{\nu\mu}(\rho)}{d\rho^2}+\left[\nu(\nu+1)-\frac{\mu^2}{\cos^2\rho}+\tfrac{1}{2}+\tfrac{1}{4}\tan^2\rho\right]H_{\nu\mu}(\rho)=0\ . \tag{14a}$$

In our region of interest, $\rho\approx 0$ and $\xi\approx 0$, so that $\nu(\nu+1)\gg\mu^2/\cos^2\rho\approx\mu^2\gg\tan^2\rho\approx\rho^2$, permitting us to write

$$\frac{d^2H_{\nu\mu}}{d\rho^2}+q^2H_{\nu\mu}=0\ , \tag{14b}$$

$$q^2\equiv\nu(\nu+1)-\mu^2+\tfrac{1}{2}\ . \tag{14c}$$

From the boundary conditions, $H_{\nu\mu}(\pm\xi)=0$, yielding

$$H_{\nu\mu}(\rho)\propto\sin[q(\xi+\rho)]\ , \tag{14d}$$

where

$$q=(n+1)\pi/2\xi=\frac{(n+1)\pi}{2\cos\alpha}\ ,\quad n=0,1,\ldots\ , \tag{14e}$$

The solutions for $H_{\nu\mu}$ are just those for a particle in an infinite square well of width 2ξ and the eigenvalue spectrum is, for $\alpha\approx\pi/2$,

$$E_{\nu\mu}\equiv\nu_{n\mu}(\nu_{n\mu}+1)\approx\epsilon(n)+\mu^2-\tfrac{1}{2}\ , \tag{15a}$$

$$\epsilon(n)\equiv[(n+1)\pi/2\cos\alpha]^2\ ,\quad n=0,1,2,\ldots\ . \tag{15b}$$

Equations (15a) and (15b) clearly demonstrate the grouping into families, each of which is characterized by a quantum number n. The spectrum within each family is characterized by μ^2, the energy of a plane rotor in a periodic azimuthal potential [see Eq. (3b)]. The quantity n is the number of zeros of P_ν^μ in the range $\alpha<\theta<\pi-\alpha$ (or $\xi>\rho>-\xi$). The number of nodes of a solution of Eq. (3c), however, is invariant as we change α. This is, perhaps, most clearly seen fron Eq. (14a), which has the form of a one-dimensional Schrödinger equation where μ^2 is interpreted as a potential parameter. For a fixed μ the sequential order of the eigenvalues, $\nu(\nu+1)$, is the same as that of the number of nodes (see Sturm's first comparison theorem[8]) independent of the value of α [even though the order of states corresponding to different μ may change, as in Fig. 3(b)]; this ordering is, of course, reflected in Eqs. (15a) and (15b). Therefore, we can classify the states by the values of μ and n for all values of the opening angle α. In the absence of modulaton and in the free rotor limit ($\alpha=0$), $n=l-m$, so that we can characterize the states by the quantum numbers m and n, and, for $\alpha\approx\pi/2$, we have in the absence of modulation,

$$E_{nm}\equiv\nu_{nm}(\nu_{nm}+1)\approx\left[\frac{\pi(l-m+1)}{2\cos\alpha}\right]^2+m^2-\tfrac{1}{2}\ , \tag{15c}$$

which corresponds to Fig. 3(b).

The partitioning of the energy in Eq. (15a) into the sum of a plane rotor (i.e., μ^2) term and a term dependent upon the number of nodes signifies the approximate separation of the motion into rotation in the midplane and motion independent of m in the polar direction (an approximation which becomes exact as $\alpha\to\pi/2$). The kinetic energy of this θ motion is a function of the number of nodes (number of oscillations for $\alpha<\theta<\pi-\alpha$) and the boundary conditions (as embodied in α). From the generality of our arguments, we expect a similar separation, in the h model, of the motion for $\alpha\approx\pi/2$ into independent degrees of freedom (i.e., motions within and perpendicular to the midplane) even if we admit nonsingular potentials dependent only on $\cos\theta$. Therefore, the grouping of the spectrum into families which are distinguished by the number of nodes n and each of which comprises the full spectrum of plane rotation (i.e., full spectrum of μ^2) as $\alpha\to\pi/2$ is expected to be general for the boundary conditions incorporated in the h model.

Interpretation of these results in terms of the degree of rotational frustration would indicate separation of the motion into the same independent degrees of freedom for any potential $W(\cos\theta)$ [see Eq. (3c)] which severely hinders the rotation in the polar direction. For different hindering potentials, however, one expects a different expression for the n-dependent energy in Eq. (15b): nevertheless, the form of Eq. (15a) is expected to be generally valid for any potential which causes severe hindrance. This point is clearly illustrated in Fig. 3(c), where we present results for $E_{nm}-E_{00}$ vs $V_1^{1/2}$ [see Eqs. (13)] for the unmodulated h_2 model (i.e., the hindrance is incorporated in the potential $V_1/\sin^2\theta$ as in the discussion of Eqs. (12) and the notation is clear from our discussion of Eqs. (15)]. The plane rotor m^2 spectrum for large V_1 is clearly manifested. The spectrum in Fig. 3(c) is described by Eqs. (13), which demonstrate the separation (as $V_1\to\infty$) into independent degrees of freedom [as in Eq. (15a) for the h model], the dependence upon $n=l-m$, and the sensitivity of the exact form of $\epsilon(n)$ to the form of the potential. Additional analysis of this model is given in the discussion following Eqs. (13) and we would like to point out the validity of the foregoing points even when

we consider azimuthal modulation of the potential energy (i.e., $\mu \neq m$, an integer), in analogy with our discussion of Fig. 3(b).

A. Azimuthal modulation

The effects of azimuthal modulation [see Eqs. (2) and (9)] are presented in Figs. 4–9. In order to make close connection with experimentally measured energy differences, we present plots of $E_{n\mu}-E_{00}$ [i.e., $E_{n\mu} \equiv \nu_{n\mu}(\nu_{n\mu}+1)$] in Figs. 5 and 7–9. To facilitate extraction of absolute energies, we give in Fig. 4 the ground-state rotational quantum numbers ν_{00} for fourfold and sixfold azimuthal symmetries [$N=4$ and 6, respectively, in Eq. (8a)] for both the h and h_2 models for the azimuthal potential parameters we use in Figs. 5–9. In Figs. 4(d)–4(f) and in Fig. 9, in which results for the h_2 model are displayed, we have chosen to exhibit our results for the energies, versus the variable $\eta \equiv \tan^{-1}(V_1^{1/4})$. This choice allows us to show results for all values of V_1 ($V_1=0$ and ∞ correspond to $\eta=0$ and $\pi/2$, respectively), and thus afford direct comparison with the corresponding results for the infinite cone-well hindrance model (the h model, where $\alpha=0$ and $\pi/2$ correspond to absence and infinite hindrance, respectively) shown in Figs. 5(a)–5(d) and 8. The choice of the specific form of the definition of η is motivated to give comparable energy differences $(E_{n\mu}-E_{00})$ in the limit of strong hindrance for the h and h_2 models [see Eqs. (13) and (15)].

In Figs. 5(a)–5(d) we present $E_{n\mu}-E_{00}$ for the h model with symmetry number $N=4$, barrier width parameter $\gamma=\epsilon/3$ and $V_1=0$, as a function of α for barrier heights $\Delta=0$ (i.e., no modulation), 5, 20, and 40: That is, progressively stronger azimuthal potentials. In each panel, a fixed number of the lowest-energy states is displayed. The effect upon azimuthal energies (μ^2) of increasing Δ [obtained by solving Eq. (10a)] is illustrated in Fig. 6 where we display k^2 [$=\mu^2$ here since $V_1=0$, see Eq. (10c)] as a function of m in the reduced zone scheme (i.e., modulus a multiple of $N/2$) for $N=4$ and 6. Note the progressively greater banding and splitting for $m=2,4,6,\ldots,$ when $N=4$ (i.e., $m=3,6,9,\ldots,$ when $N=6$) as we increase the height of the barrier Δ.

The banding shown in Fig. 6 is clearly reflected in the energies displayed in Fig. 5. This banding is reflected

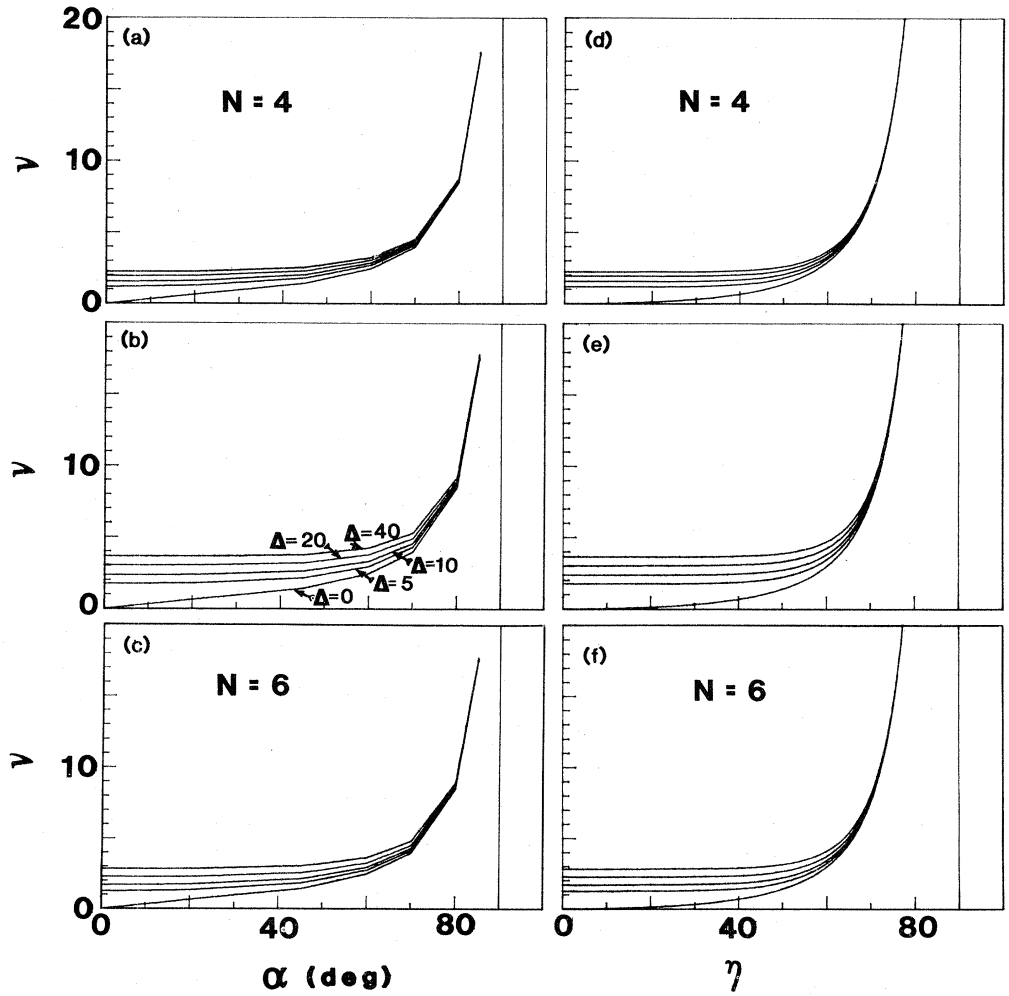

FIG. 4. Rotational quantum numbers ν for the ground states of the h [i.e., (a)–(c)] and h_2 [i.e., (d)–(f)] hindrance models vs the angles α and $\eta \equiv \tan^{-1}(V_1^{1/4})$, in degrees, respectively, for various azimuthal modulation barrier heights [indicated in panel (b)]. Results for fourfold symmetry ($N=4$) are exhibited in (a), (b), (d), and (e) with barrier width parameters $\gamma=\epsilon/3$ and $\gamma=2\epsilon/3$ corresponding to (a) and (d) and (b) and (e), respectively. (c) and (f) display sixfold symmetry results with $\gamma=\epsilon/3$.

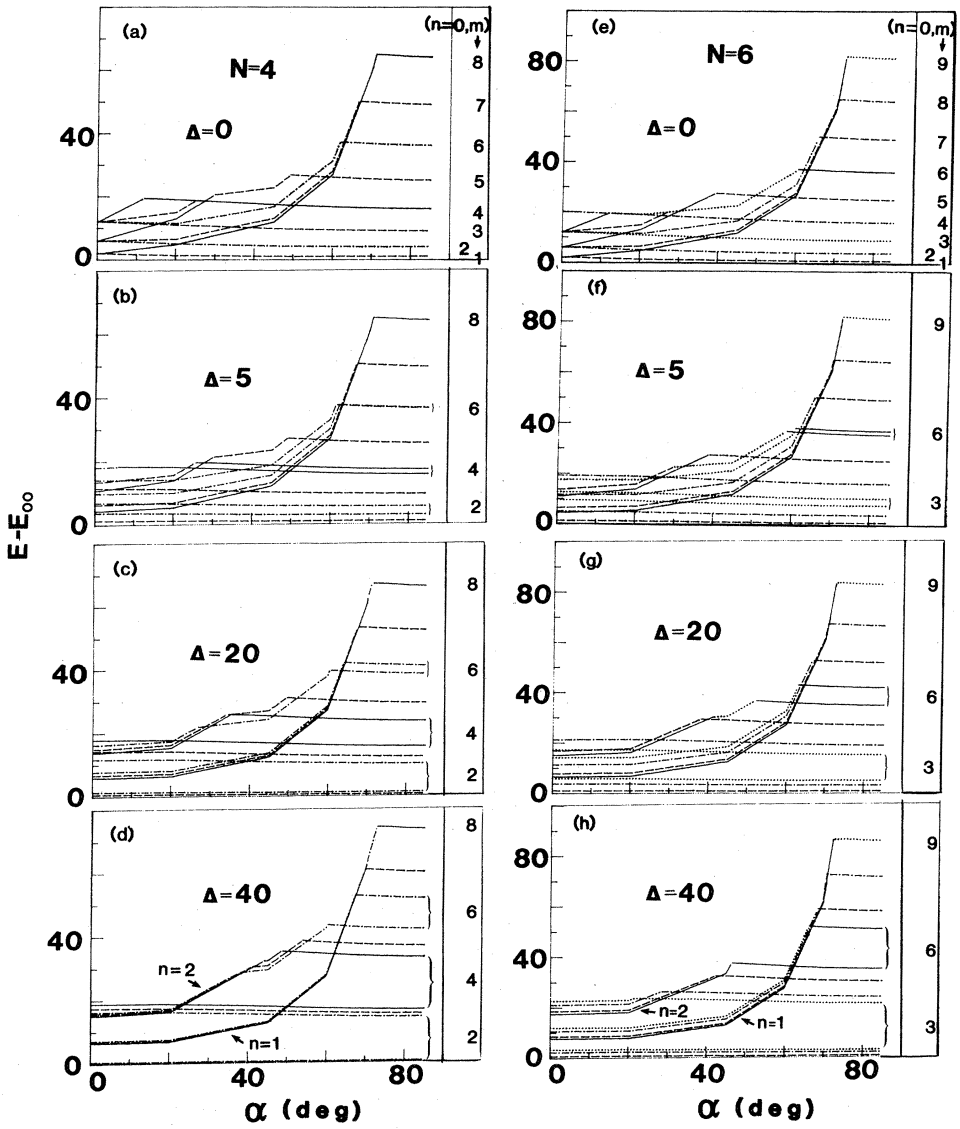

FIG. 5. Effect of azimuthal modulation on the energy differences $E-E_{00}$ (in units of $\hbar^2/2I$) for horizontally hindered rotors (h model) of symmetry numbers $N=4$ [i.e., (a)–(d)] and $N=6$ [i.e., (e)–(h)]. In all calculations $V_1=0$ and the barrier width $\gamma=\epsilon/3$. The unmodulated spectra are shown in panels (a) and (e) and spectra for successively larger modulation barriers are shown as follows: $\Delta=5$ in (b) and (f); $\Delta=20$ in (c) and (g); and $\Delta=40$ in (d) and (h). In each case the (n,m) designation for the $n=0$ family is shown with m being the azimuthal quantum number in the limit of vanishing modulation. The convergence of states into bands upon increasing modulation strength is clearly seen. The band gaps due to the periodic azimuthal modulation (see Fig. 6) are indicated by curly brackets on the right of each panel along with the corresponding m quantum numbers. For large hindrance (α) and in the absence of modulation the states within each family exhibit a plane rotor spectrum [shown clearly in the $n=0$ families in panels (a) and (e)]. In the presence of modulation and for large hindrance the separation between consecutive states (in each family) obey Eqs. (16). States belonging to the $n=1$ and 2 families are indicated in (d) and (h).

within each of the families discussed earlier. The limiting form in Eq. (15a) describes the energies in the high-α regime. It is interesting to observe from Fig. 5 that this form is valid over a larger range of hindrance angles than one might expect from the derivation of Eq. (15a), which indicates that the separation into independent degrees of freedom discussed in connection with Eqs. (15) (one involving only n and the other only μ), is valid over a rather large range of hindrance angles α. Note that the size of the angular range of validity of Eq. (15a) decreases with increasing energy. In this angular range, the energy difference of two states characterized by the same value of n (i.e., belonging to the same family) is

$$E_{n\mu_2}-E_{n\mu_1}=\mu_2^2-\mu_1^2=k_2^2-k_1^2\ , \tag{16a}$$

in particular,

$$E_{0\mu}-E_{00}=\mu^2-\mu_0^2=k^2-k_0^2\ , \tag{16b}$$

where μ_0^2 and k_0^2 correspond to the lowest band energy. The energy difference of states of different n diverges as $\alpha\rightarrow\pi/2$, of course.

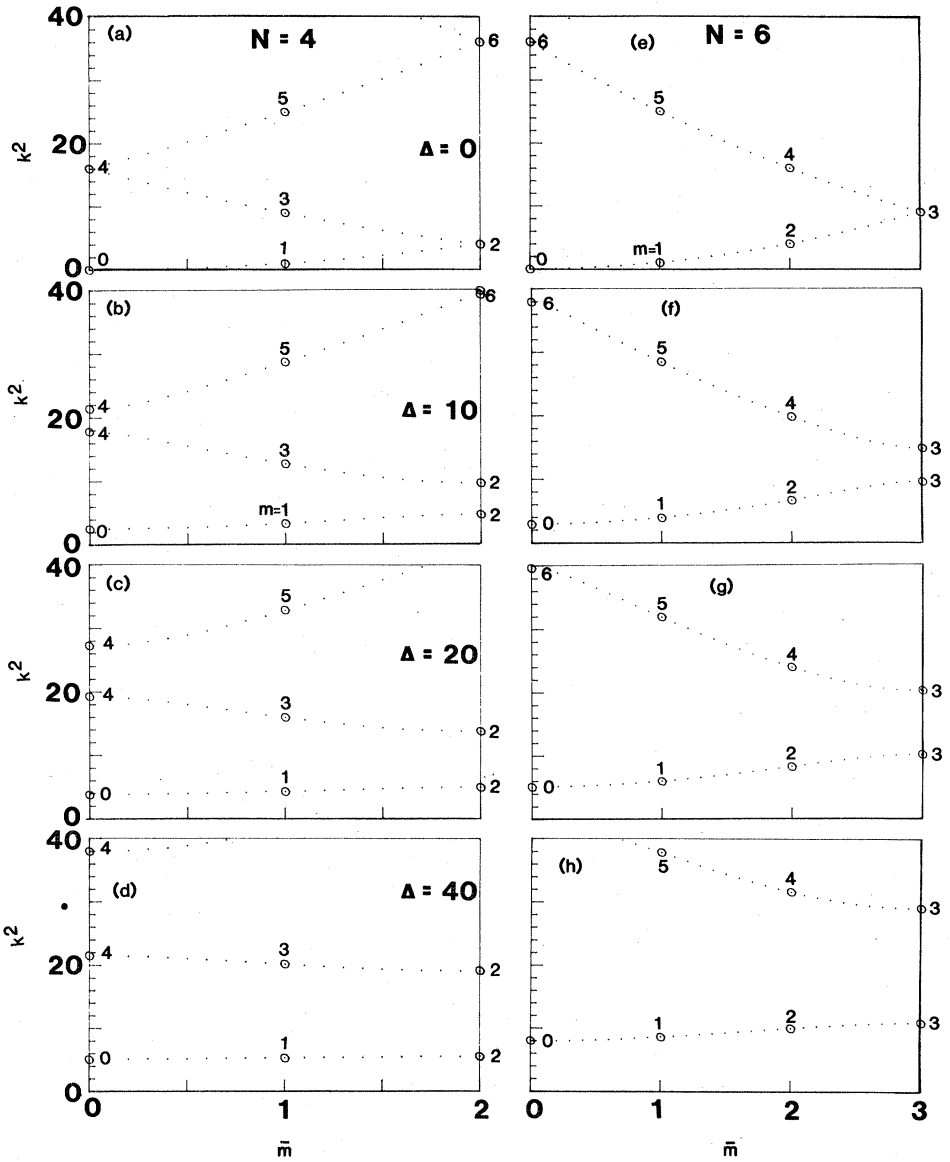

FIG. 6. Band structure (k^2 vs m) corresponding to the Kronig-Penney periodic azimuthal modulation potential (see Fig. 2) for fourfold and sixfold periodicities [$N=4$ in (a)–(d) and $N=6$ in (e)–(h), respectively], in the absence of modulation [(a) and (e)] and for increasing barrier heights: $\Delta=10$ in (b) and (f); $\Delta=20$ in (c) and (g) and $\Delta=40$ in (d) and (h). In all calculations $V_1=0$ and $\gamma=\epsilon/3$. The reduced zone scheme is used; $\bar{m}=2$ and 3 are the first Brillouin-zone edges for $N=4$ and 6, respectively. The values of k^2 were obtained via solution of Eq. (10a) and are denoted by circles. The numbers alongside the circles give the value of m (i.e., extended zone scheme) to which μ corresponds. Note the opening of band gaps at the Brillouin-zone edges which become wider along with a flattening of the dispersion upon increasing modulation barrier height Δ.

In the unhindered ($\alpha=0$ and $V_1=0$) limits of the h and h_2 models, the energies can be calculated from Eq. (7a). The equations corresponding to Eqs. (16) are in this case

$$E_{n\mu_2}-E_{n\mu_1}=\mu_2^2-\mu_1^2+(2n+1)(\mu_2-\mu_1)$$
$$=k_2^2-k_1^2+(2n+1)(k_2-k_1)\,, \tag{17a}$$

and

$$E_{n\mu}-E_{00}=k^2-k_0^2+(2n+1)k-k_0+n(n+1)\,, \tag{17b}$$

$$E_{0\mu}-E_{00}=k^2-k_0^2+(k-k_0)\,. \tag{17c}$$

It is evident from Fig. 5 that the variation in the plotted energy differences for the $n=0$ family is slow across the whole range of hindering cone angle α; if we could, therefore, isolate the contribution of this family to the experimental spectra, we could expect to be able to extract the azimuthal band structure (k^2 spectrum) by some interpolation technique. In either of the limiting regimes discussed above, our program of azimuthal band-structure extraction should proceed without serious complications. In the intermediate angular (hindrance) regime, however, isolation of the $n=0$ family is complicated by the presence of levels corresponding to nonzero values of n: that is, level crossing. In fact, the seeming slope discontinui-

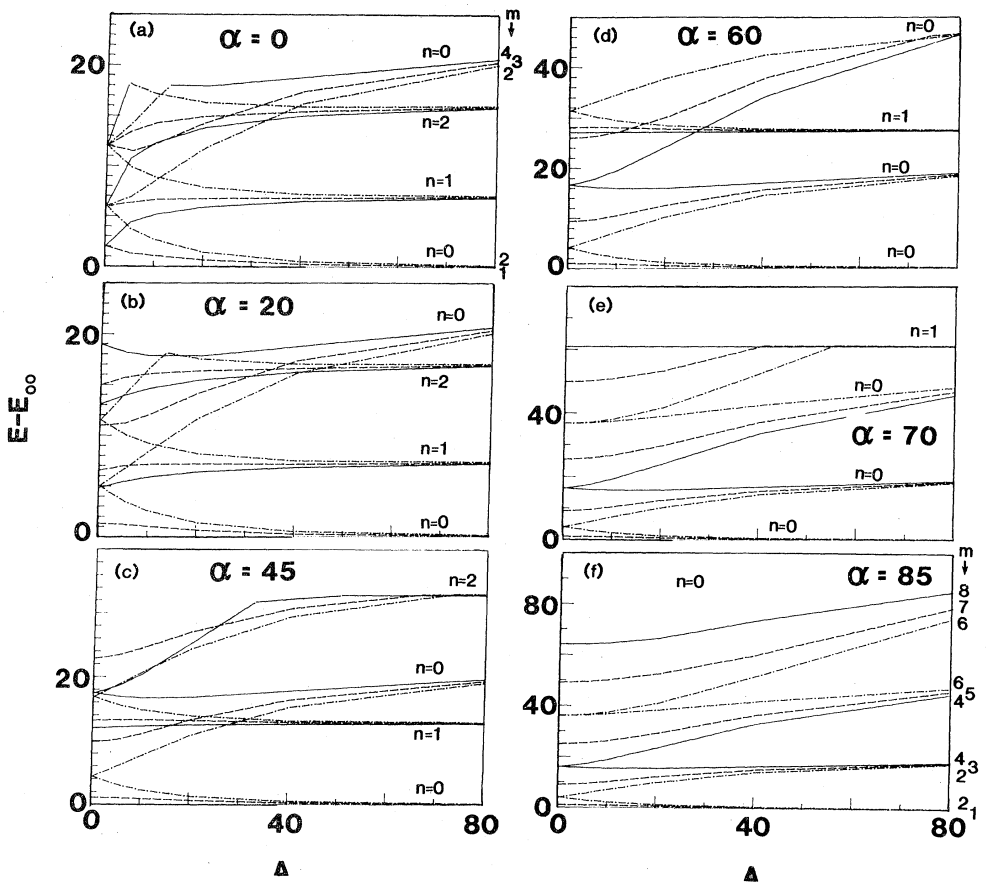

FIG. 7. Energy differences $E-E_{00}$ (in units of $\hbar^2/2I$) for the horizontally modulated hindered rotation model (h model) as a function of the azimuthal modulation barrier height Δ in the absence of hindrance ($\alpha=0$) in (a) and for increasing hindrance [$\alpha=20$, 45, 60, 70, and 85, in degrees, corresponding to panels (b)—(f), respectively] for fourfold periodicity ($N=4$). In all calculatons $V_1=0$ and $\gamma=\epsilon/3$. The different families in the spectra are indicated by their n values. The m values for the $n=0$ family are shown in (a) and (f). The grouping of the states into well-defined bands upon increasing modulation strength is evident. The range of Δ's for which a clear separation of bands is possible increases upon increasing hindrance strength. The increase in the energies of states belonging to $n\neq 0$ families is exhibited.

ties of the energies in Fig. 5 arise because, for graphical simplicity, we consider a fixed number of lowest energy states for each α: level crossing produces the appearance of discontinuities in the slope.

The effect of increasing the barrier width γ is to increase the energies of the states. For a given value of γ, increasing the barrier height Δ can increase the number of bound states which the well can support [$k^2<\Delta$, see Eq. (10)] and for these states the bands become narrower and the band gaps wider. Note, however, that for the unbound part of the spectrum ($k^2>\Delta$) the above rule is not necessarily obeyed.

We should note that the spectrum becomes progressively simpler as the band effects become stronger [e.g., compare Figs. 5(a) and 5(d)]. This effect is clearly manifested in Fig. 7, where we present $E_{n\mu}-E_{00}$ for the h model, $N=4$ and $\gamma=\epsilon/3$ as a function of Δ for different values of α. The spectrum simplifies for large modulating potentials (large Δ), and in the extreme limits of hindrance [$\alpha\rightarrow 0$, Fig. 7(a) and $\alpha\rightarrow\pi/2$, Fig. 7(f)]. For these situations, we expect to be able to extract information regarding the azimuthal motion without major difficulties. Even in the regime of intermediate hindrance and intermediate azimuthal band-structure effects, it is possible to use these systematics to formulate a prescription for data analysis. We postpone discussions of the procedure until the end of this section.

An illustration of the azimuthal band-structure effects observable in the spectrum is given in Fig. 7(f), which corresponds to $\alpha=85°$ (i.e., high hindrance). As we increase Δ the opening of gaps at the Brillouin-zone boundaries (i.e., even values of m for $N=4$) is evident. As we decrease α (i.e., lower the degree of hindrance), we see that the higher energy states are the first to exhibit the complications produced by level crossing for intermediate values of Δ. Note, for example, that the levels of the lowest band retain their simplicity at least until $\alpha=45°$.

Another clear feature of Fig. 7 is the behavior of the families corresponding to different n with increased hindrance (increasing α). As we increase α, the $n\neq 0$ bands rise with respect to the others, until, in Fig. 7(c), the $n=2$ band is the highest band [i.e., compare with Fig. 5(e)]. With further increase of α, the $n\neq 0$ bands rise even more, until, for $\alpha=60°$, the $n=2$ band has risen above a third $n=0$ band, and the $n=1$ band has become the third highest in Fig. 7(d). At 70°, only $n=0$ bands appear in

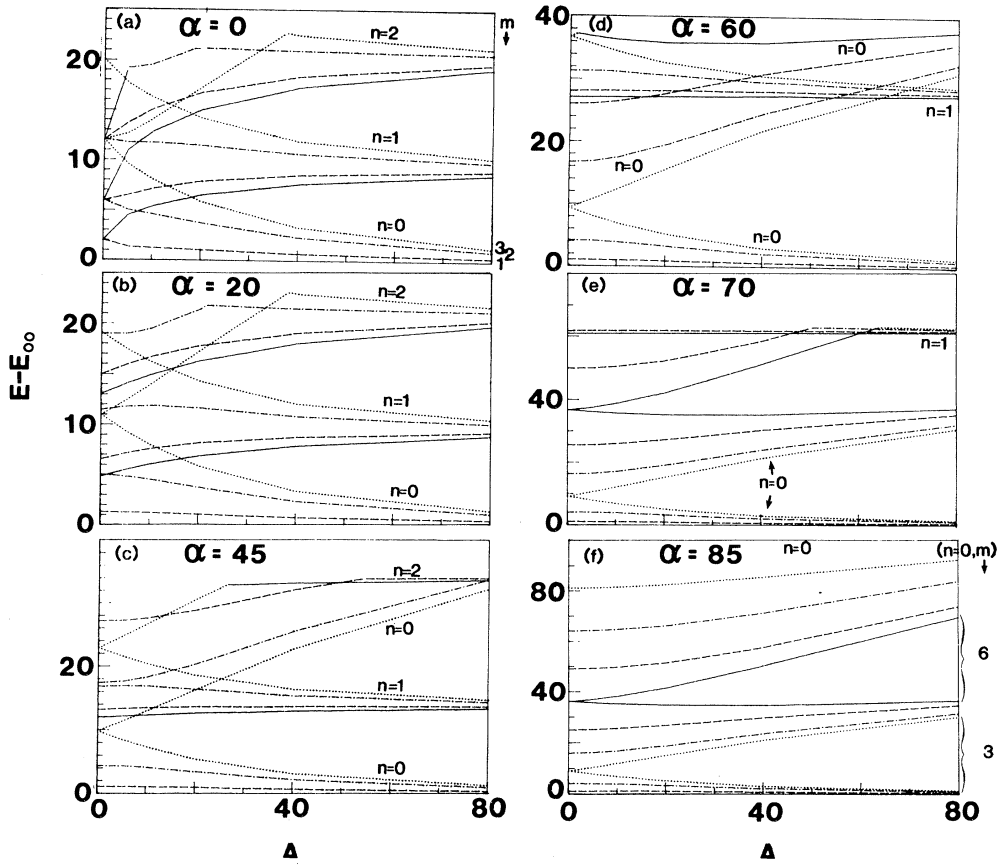

FIG. 8. Energy differences $E-E_{00}$ for the horizontally modulated hindered rotation model (h model) as a function of the azimuthal modulation barrier height Δ for sixfold periodicity ($N=6$). See caption to Fig. 7.

Fig. 7(e); also see Eqs. (15).

Figures 5(e)—5(h) and 8 correspond to Figs. 5(a)—(5(d) and 7, respectively, for the h model, where the azimuthal modulating potential possesses a sixfold symmetry (i.e., $N=6$). Except for such details as the position of the Brillouin zone edge (i.e., the gaps occur at multiples of 3 in this case), the discussion of Figs. 5 and 7 is adequate to describe these spectra.

Finally, in Fig. 9, we present $E_{n\mu}-E_{00}$ for the h_2 model for $N=4$ and $\gamma=\epsilon/3$. In Figs. 9(a)—9(c) we show results for the energy differences versus $\eta\equiv\tan^{-1}(V_1^{1/4})$ for azimuthal barrier heights $\Delta=0$, 10, and 40, respectively, while results plotted versus the modulation barrier height Δ for selected values (0, 10, and 1000 or $\eta=0°$, 60°, and 80°, respectively) of V_1 (which controls the degree of hindrance) are shown in Figs. 9(d)—9(e). The results in Figs. 9(a) and 9(c) correspond to Figs. 5(a) and 5(d) for the other hindrance model (h model), respectively. The results shown in Figs. 9(d) and 9(e) for intermediate and large values of V_1 correspond, respectively, to the results for intermediate values of α which controls the degree of hindrance in the h model, shown in Figs. 7(c) and 7(d).

In the unhindered, or $V_1=0$, limit of the h_2 model, the energies are given by Eqs. (17). We can write the exact expressions for the energy for this model for general V_1. From Eqs. (7a) and (10c), we have

$$E_{n\mu_2}-E_{n\mu_1}=k_2^2-k_1^2+(2n+1)(\mu_2-\mu_1)\,, \tag{18a}$$

$$\mu_i=(V_1+k_i^2)^{1/2}\,, \tag{18b}$$

$$E_{n\mu}-E_{00}=k^2-k_0^2+(2n+1)\mu-\mu_0+n(n+1)\,, \tag{18c}$$

$$E_{0\mu}-E_{00}=k_2-k_0^2+\mu-\mu_0\,. \tag{18d}$$

The quantity μ_0 represents the lowest $m=0$ band state. In the limit $V_1\to\infty$, the energy differences are identical to those corresponding to the h model for $\alpha\to\pi/2$ given in Eqs. (16), illustrating the separation into independent degrees of freedom [i.e., see the discussion of Fig. 3(c)].

In Fig. 9, we observe the same systematics as discussed in connection with Fig. 5. In particular, it is shown that the energy differences between states of a given n family have identical forms for the h and h_2 models in the unhindered and high hindrance limits. Furthermore, the variation of these energy differences due to varying the degree of hindrance is smooth. Although the variation is slowest (i.e., almost constant) for the $n=0$ family, it is still quite slow for the low $n\neq0$ families.

From the similarity of these systematics of the h and h_2 models, which correspond to different hindering potentials, we expect them to be general for any separable hindering potential. For motives of data analysis, therefore, it is sufficient to utilize Eqs. (18) to represent the variation with frustration (even though the energies in the

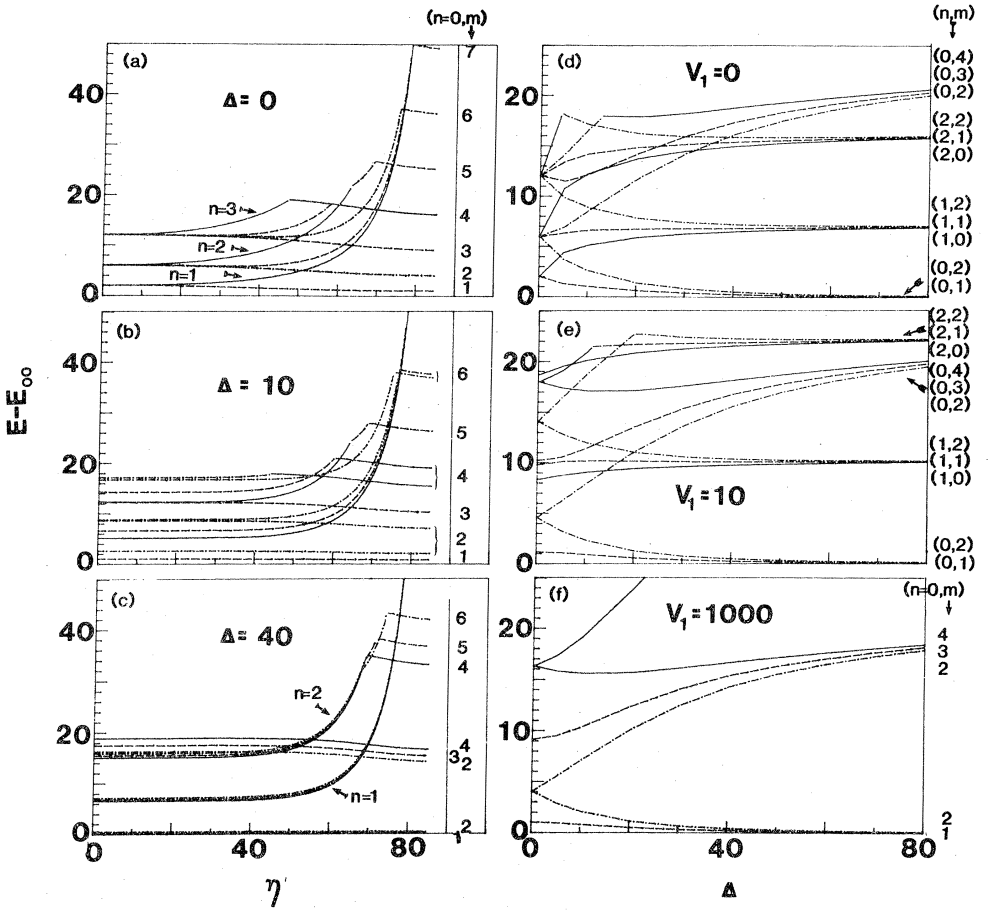

FIG. 9. (a)—(c) Energy differences $E-E_{00}$ (in units of $\hbar^2/2I$) for the h_2 hindrance model vs $\eta=\tan^{-1}(V_1^{1/4})$ (in degrees) in the absence of azimuthal modulation [$\Delta=0$ in (a)] and for intermediate and large modulation barrier heights [$\Delta=10$ and 40 in (b) and (c), respectively]. Different families are indicated and the m designation of states in the $n=0$ family is given. The similarity of the spectra to those shown in Fig. 5 (corresponding to the h hindrance model) is evident. (d)—(f) Energy differences $E-E_{00}$ for the h_2 hindrance model vs modulation strength Δ in the absence [$V_1=0$ in (d)] and for intermediate [$V_1=10$ in (e)] and high [$V_1=1000$ in (f)] values of the hindering parameter V_1 of the h_2 model. The classification of the states by (n,m) is indicated on the right of each panel. Note the similarity of the behavior of the spectra with increasing hindrance (V_1) to those in Fig. 7 for the h hindrance model.

h model could be parametrized from, for example, Figs. 5 and 7).

B. Data reduction scheme

From these considerations, we can suggest a prescription for data analysis.

(a) A complete assignment of the states and analysis in terms of model potentials requires a large data base. Without information regarding the energies of the $n\neq0$ families, it is not possible, in general, to unambiguously determine both the band structure and the hindering potential.

(b) Determination of the site symmetry (i.e., N) should be made via independent experiments (such as low-energy electron diffraction, high resolution vibrational EELS, or other methods). In principle, in the presence of strong band effects the site symmetry may be determined (as in Figs. 5 and 7—9).

(c) Parametrization of the energy differences; as we have discussed, Eqs. (18) provide an adequate parametrization in the absence of independent information concerning the hindering potential.

(d) Determination of the hindrance-modulation regime:

(i) If the experimental spectrum displays[12] well-separated bands, we are in the severe hindrance regime and the band struture (i.e., μ^2) can be extracted without difficulty (although exact determination of the hindering potential is not possible).

(ii) If, on the other hand, the spectra manifest well-defined bands, all of which are not necessarily cleanly separated, as in the intermediate range in Figs. 5(c) and 5(f), for example, we have the *strong azimuthal band effect* regime [there is obviously an overlap between regimes (i) and (ii)]. In this regime, assignment of the values of n is straightforward and the data can be analyzed from the consistency relations embodied in Eqs. (18).

(iii) The *intermediate* regime (moderate hindrance and modulation) is the most difficult to analyze because the spectra present neither well-defined bands nor well-separated lines. In this case, it is necessary to tentatively identify the n values to which the spectra correspond, with

the aid of the systematics exhibited in Figs. 5–9. The lowest $n=0$ and 1 bands, for example, must be consistently related, as in Eqs. (18). The resulting parameter values must obey Eq. (18c) for the lowest $n=2$ band. If this final step is violated, the n values of the spectra must be reassigned. This discussion clarifies the reason for measuring as many $n\neq 0$ spectra as possible.

IV. SUMMARY

We have studied the rotational states of an admolecule for different adsorption configurations and for different types and degrees of hindrance and azimuthal modulation of the molecular motion. For a molecule whose equilibrium adsorption configuration is parallel to the surface, we have considered an infinite conical-well hindrance (the h model) and a hindering potential which prevents the molecule from assuming a vertical configuration in a gradual manner (the h_2 model). In addition to the above hindrance models of motion in the polar angle direction, we investigated an azimuthal modulation of the molecular motion with a periodicity dependent upon the adsorption site local symmetry. In the case of a molecule bound to the surface in a vertical equilibrium configuration (the v model) only the infinite cone-well hindrance was considered.

Common to all the model systems which we have studied is the raising of the energy of the rotational states due to hindrance and/or modulation potentials which act to spatially confine the system. Examination of the solution for the h model in the regime of strong hindrance led us to a classification of the rotational states of the system in terms of quantum numbers n and μ where n is the number of zeros of the wave function $P_\nu^\mu(\cos\theta)$ for the polar motion and μ characterizes the azimuthal motion of the rotor. For an unhindered rotor $\nu\rightarrow l$ and in the absence of modulation $\mu\rightarrow m$ such that $n=l-m$. The partitioning of the rotational energy into contributions from the polar motion (characterized by n) and planar rotation (characterized by μ), which becomes exact for large hindrance, is shown to hold for any potential which introduces severe frustration. This separation forms the basis for the general classification scheme in which the rotational states are grouped according to n and within each group exhibit a manifold of states characterized by μ. This classification scheme allows us to correlate states between the limits of weak and strong hindrance.

Effects due to azimuthal modulation of the admolecule's motion were studied by us via a simple Kronig-Penney potential model which possesses the adsorption site symmetry (i.e., dependent upon the substrate atomic arrangement in the vicinity of the adsorbed molecule). In this model the index μ is a solution to a characteristic transcendental equation [Eq. (10)] which depends on the potential parameters [the base potential V_1, height and width of the barriers (Δ and γ, respectively) and the symmetry number N (see Fig. 2)]. The solutions of Eq. (10) provide the azimuthal rotation band structure (see Fig. 6). We observed banding of the rotational states, for hindered rotors, which occurs within each of the spectral families (indexed by n) and is pronounced over a range of hindrance and modulation strengths (in the limit of large modulation barriers the solution for a particle in an infinite square well of width 2γ is reached).

The generality of our arguments concerning the effects of the hindering potential and the periodic azimuthal modulation as well as the similarity of the numerical results for the model hindering potentials we consider (which differ in the manner in which they influence the molecular motion), lead us to believe that the overall characteristics, the classification scheme, and the spectroscopic consequences of our models will be manifested in investigations employing more elaborate interaction potentials (when available).

Based on the above observations we suggest a data-reduction scheme, summarized at the end of Sec. III, which could be used for the classification and analysis of future experimental data and provide guidelines for the extraction of information about the character of the admolecule motion and the degree of its hindrance and modulation by the interaction with the substrate.

ACKNOWLEDGMENTS

This work was supported by the U. S. Department of Energy under Contract No. EG-S-05-5489. One of us (G.G.K.) would like to thank Conselho Nacional de Pesquisas (Brasil) for partial support.

---

*Permanent address: Institute de Física, Universidade Estadual de Campinas, 13100 Campinas, São Paulo, Brazil.

[1]Ph. Avouris, D. Schmeisser, and J. E. Demuth, Phys. Rev. Lett. 48, 199 (1982); S. Anderson and J. Harris, *ibid.* 48, 545 (1982).

[2]H. Ibach, Sur. Sci. 66, 56 (1977); E. W. Plummer, W. Ho, and S. Andersson in *Aspects of the Kinetics and Dynamics of Surface Reactions (LaJolla Institute, 1979),* Proceedings of the Workshop on Aspects of the Kinetics and Dynamics of Surface Reactions edited by Uzi Landman (AIP, New York, 1980).

[3]I. F. Silvera and M. Nielsen, Phys. Rev. Lett. 37, 275 (1976); R. R. Cavanagh, R. D. Kelley, and J. J. Rush, J. Chem. Phys. 77, 1540 (1982).

[4](a) A. W. Kleyn, A. C. Luntz, and D. J. Auerbach, Phys. Rev. Lett. 47, 1169 (1981); F. Frenkel, J. Hager, W. Krieger, H. Walter, C. T. Campbell, G. Ertl, H. Kuipers, and J. Seger, *ibid.* 46, 152 (1981); R. R. Cavanagh and D. S. King, *ibid.* 47, 1829 (1981). (b) L. Efstathiou and E. W. Thomas, Nucl. Instrum. Methods 194, 589 (1982); E. W. Thomas and L. Efstathiou, *ibid.* (in press).

[5]For a review see A. J. Barnes, *Vibrational Spectroscopy of Trapped Species* (Wiley, New York, 1973); A model for hindered rotations in crystalline solids was given originally by L. Pauling, Phys. Rev. 36, 430 (1930). Studies in this field explore the vibration and rotational spectroscopy of molecules trapped in solids and the vibrational relaxation mechanisms of the trapped molecular species via its coupling to the host. For

recent work see H. Kono and S. H. Lin, J. Chem. Phys. 78, 2607 (1983), and references cited therein; M. Berkowitz and R. B. Gerber, Chem. Phys. 37, 369 (1979).

[6]J. W. Gadzuk, U. Landman, E. J. Kuster, C. L. Cleveland, and R. N. Barnett, Phys. Rev. Lett. 49, 426 (1982); J. Electron Spectrosc. Relat. Phenom. 30, 103 (1983); U. Landman, Israel J. Chem. 22, 339 (1982).

[7]D. White and E. N. Lassettre, J. Chem. Phys. 32, 72 (1960).

[8]P. M. Morse and H. Feshbach, *Methods of Theoretical Physics* (McGraw-Hill, New York, 1953), Vol. 1.

[9]R. de L. Kronig and W. G. Penney, Proc. R. Soc. London Ser. A 130, 499 (1931).

[10]H. Eyring, J. Walter, and G. E. Kimball, *Quantum Chemistry* (Wiley, New York, 1944), p. 75.

[11](a) A. Sommerfeld and H. Hartmann, Ann. Phys. 37, 333 (1940); (b) H. Muller, Wiss. Z. Friedrich-Schiller-Univ. Jena, Math.-Naturwiss. Reihe 25, 745 (1976).

[12]As discussed in Sec. III in the absence of hindrance and modulation the spectra consist of sharp lines. Upon turning on of hindrance and modulation interactions degeneracies are lifted and banding occurs which would exhibit itself as a broadening of the transitions (see, for example, Figs. 5–9). At the high modulation and/or hindrance limits the spectra simplify again turning into narrow lines.